Electronic Raman scattering in $HgBa_2Ca_2Cu_3O_{8+\delta}$ single crystals: Analysis of the superconducting state

A. Sacuto
Laboratoire de Physique de la Matière Condensée, Ecole Normale Supérieure, 24 rue Lhomond, 75005 Paris, France

R. Combescot
Laboratoire de Physique Statistique, Ecole Normale Supérieure, 24 rue Lhomond, 75005 Paris, France

N. Bontemps and C. A. Müller
Laboratoire de Physique de la Matière Condensée, Ecole Normale Supérieure, 24 rue Lhomond, 75005 Paris, France

V. Viallet and D. Colson
Physique de l'Etat Condensé DRECAM/SPEC, CEA, Saclay, 91191 Gif-sur-Yvette, France

(Received 6 April 1998)

Electronic Raman-scattering measurements have been performed on $HgBa_2Ca_2Cu_3O_{8+\delta}$ single crystals in the superconducting state. Pure electronic Raman spectra with no phonon structures hindering the analysis of the electronic continuum have been obtained. As a consequence, the spectra in the pure B_{1g} and B_{2g} symmetries are directly and reliably analyzed and the pure A_{1g} contribution can be easily identified. Below the critical temperature T_c, two electronic structures at $2\Delta \sim 6.4\ k_B T_c$ and $2\Delta \sim 9.4\ k_B T_c$ are clearly seen. Both are observed simultaneously in pure A_{1g} symmetry, the highest energy one being located at the energy of the B_{1g} maximum. These two maxima disappear at T_c and do not soften significantly as the temperature is raised up to T_c. The low-energy frequency dependence of the B_{1g} electronic response is strongly linear, for various excitation lines in the 476.5–647.1 nm range. Such experimental data cannot be reconciled with a pure $d_{x^2-y^2}$ symmetry. Instead, they strongly advocate in favor of an anisotropic superconducting gap with two distinct gap maxima and of nodes existing outside the [110] and $[1,\bar{1},0]$ directions in **k** space. We discuss in detail the simplest order parameter compatible with our experimental findings. [S0163-1829(98)00238-0]

I. INTRODUCTION

Since the last few years, identifying the symmetry of the pairing state has been the expected major step towards an understanding of high-T_c superconductivity. The controversy is not yet resolved: while there seems to be an agreement on the existence of nodes in the gap, some experiments appear to advocate in favor of a pure $d_{x^2-y^2}$ symmetry,[1] whereas others seem to exhibit a significant *s*-wave contribution.[2] With respect to this problem, inelastic light scattering has been shown very early to be a powerful tool because, besides probing the bulk (in contrast with photoemission and tunneling), the polarization selection rules on the incident and scattered light make the spectra sensitive to the wave-vector of the electronic excitations.[3–6] A theoretical approach of electronic Raman scattering has been developed, in the case of $d_{x^2-y^2}$ symmetry. The emphasis is put on the low-energy spectrum, which is expected in this case to exhibit well-defined power laws, according to the symmetry channel, e.g., the polarization of the incoming and outgoing light. More precisely, the so-called A_{1g} and B_{2g} symmetry should display a linear dependence versus frequency, as these channels are sensitive to the nodes in the $k_x = k_y$ direction, whereas the B_{1g} symmetry probes mainly directions around the $k_x = 0, k_y = 0$ directions and should display a ω^3 frequency dependence.[6] Such calculations omit other excitations such as phonons. The experimental major difficulty lies then in the fact that in most investigated compounds, e.g., $La_{2-x}Sr_xCuO_4$, $YBa_2Cu_3O_{7-\delta}$ (Y-123), $Bi_2Sr_2CaCu_2O_{8+\delta}$ (Bi-2212), and $Tl_2Ba_2CuO_{6+\delta}$ (Tl-2201), a large phonon contribution is superimposed to the electronic excitations in particular at low frequency and has therefore to be subtracted, which precludes an accurate determination of the shape of the electronic contribution in the superconducting state.[7–15] Despite this difficulty, in a number of papers, satisfactory agreement is claimed to be found between the electronic response obtained after subtraction of the phonon lines, and the $d_{x^2-y^2}$ model.[6,12,14]

In this work, we report *pure* electronic Raman spectra in $HgBa_2Ca_2Cu_3O_{8+\delta}$ (Hg-1223) single crystals, belonging to the highest-T_c cuprate family. This provides a large spectral range below the superconducting gap frequency where the low-energy electronic spectrum can be analyzed. Moreover, within this range, no subtraction of the phonons is required to discuss the electronic response.[16] Indeed, as shown in our previous work,[16–18] the very low intensity of the Raman phonon peaks for electric fields within the CuO_2 planes allows a reliable analysis of the electronic excitations in the superconducting state. The crystallographic structure of Hg-1223 is tetragonal ($^1D_{4h}$),[19] which yields an unambiguous comparison with theoretical calculations based on tetragonal symmetry, without the complications due to the orthorhombic distortion as in Y-123.[15] Hg-1223 is therefore particularly well suited for the study of the electronic Raman scattering. Our

most striking results are (i) the existence of two electronic maxima at $2\Delta = 6.4\ k_B T_c$ and $2\Delta = 9.4\ k_B T_c$, both detected in A_{1g} symmetry. These two maxima disappear at T_c. (ii) the low-frequency behavior of the B_{1g} spectrum displays what we believe to be an intrinsic linear term, which is observed for all excitation energies used in this work (476.5–647.1 nm spectral range). Such observations imply that the gap is strongly anisotropic with two distinct maxima and that nodes exist outside the [110] and $[1,\overline{1},0]$ directions. We argue that our results, which are at odds with a pure $d_{x^2-y^2}$ gap symmetry, imply an order parameter with two maximum gap values and eight nodes.

II. ELECTRONIC RAMAN SCATTERING IN THE FRAMEWORK OF BCS THEORY

We briefly recall the standard theoretical framework for electronic Raman scattering that we will use in the analysis of our experimental results.[3] Electronic Raman scattering is a process of inelastic light scattering where an incident photon is absorbed by the crystal and a scattered one is emitted, with the simultaneous creation (Stokes) or annihilation (anti-Stokes) of an electronic excitation. Here we will only have to deal with Stokes processes. Since two photons are coming into play, Raman scattering is a second-order process in the electromagnetic field. This second-order effective interaction with electronic excitations comes both from a direct second-order term in the interaction Hamiltonian, and from a first-order term treated up to second order in perturbation. As introduced by Abrikosov and Genkin,[4] one may consider that both terms can be gathered in a single effective second-order term in the Hamiltonian that can be written as

$$H_R = \frac{e^2}{m}\langle A_S A_L\rangle e^{-i\omega t}\hat{\rho}_q, \tag{1}$$

where e is the electronic charge and m its bare mass. A_L and A_S are the vector potentials of the incoming laser and scattered light, and the bracket is for the proper matrix element over the photons states. The difference between the incident and the scattered photon frequencies is noted $\omega = \omega_L - \omega_S$, and the difference between the photon momenta is $\mathbf{q} = \mathbf{k}_L - \mathbf{k}_S$. The operator $\hat{\rho}_q$ is given by

$$\hat{\rho}_q = \sum_{n_f, n_i, \mathbf{k}} \gamma_{n_f, n_i, \mathbf{k}} c^+_{n_f, \mathbf{k}+\mathbf{q}} c_{n_i, \mathbf{k}}. \tag{2}$$

It is quite similar to the standard density operator, the only difference being the $\gamma_{n_f, n_i, \mathbf{k}}$ for the scattering process, known as the Raman vertex, which is given explicitly by

$$\gamma_{n_f, n_i, \mathbf{k}} = \mathbf{e}_S \cdot \mathbf{e}_L \delta_{n_f, n_i} + \frac{1}{\hbar m}\sum_{n_m} \frac{\langle n_f, \mathbf{k}+\mathbf{q}| e^{-i\mathbf{k}_S\cdot\mathbf{r}} \mathbf{e}_S\cdot\mathbf{p}| n_m, \mathbf{k}+\mathbf{k}_L\rangle \langle n_m, \mathbf{k}+\mathbf{k}_L| e^{i\mathbf{k}_L\cdot\mathbf{r}} \mathbf{e}_L\cdot\mathbf{p}| n_i, \mathbf{k}\rangle}{\varepsilon_{n_i,\mathbf{k}} - \varepsilon_{n_m,\mathbf{k}+\mathbf{k}_L} + \omega_L + i\eta} + (L \leftrightarrow S). \tag{3}$$

It is quite important that this Raman vertex has a **k** dependence, otherwise electronic Raman scattering would essentially vanish, for symmetry reasons in B_{1g} and B_{2g} symmetry, and because of screening in A_{1g} symmetry.

The interest of the reduced form in Eq. (2) is that we have to deal only with electrons in a single band. In particular, when the photon energies ω_L and ω_S are neglected in the denominator of Eq. (3), it can be shown that the Raman vertex is identical to the contraction of the **k** -dependent inverse effective mass tensor of this band with the polarization vectors of the incident and the scattered light. This latter reduced formula is sometimes used to make explicit calculations of the Raman vertex from an assumed knowledge of the band structure. In general, a single band is assumed at the Fermi level. It is not obvious at all that this is reasonable in high-T_c compounds, although one may argue that the Raman process is dominated by a single band (this is strongly suggested by the similarity of electronic Raman scattering between various high-T_c superconductors).

Moreover, the effective mass formula assumes that the energy of all the states belonging to other bands are far enough from the Fermi level in order to neglect the photon energies in the denominator. While this approximation is reasonable for simple metals (one band is near the Fermi level and the other bands are far away), it appears much more doubtful in high-T_c superconductors. In particular, it is known that the absorption is important at the incident frequency, linked to interband transitions. This invalidates the approximation of neglecting the photon energies and implies instead the existence of resonant terms. This is actually coherent with what we observe experimentally, since the electronic Raman scattering varies in an important way as a function of the incident photon energy (as we will see in Sec. V B). Moreover, in order to deal consistently with these quasiresonant terms, we have to take into account the finite lifetime of the highly excited intermediate states. We expect, on the basis of optical data, that this relaxation rate is large, of order of a few tenths of eV. All this makes it clear that the effective mass approximation is not valid in our experimental situation. Therefore, we will rather consider that the Raman vertex is actually an effective quantity that depends not only on the wave vector **k**, but also on the incident and scattered photon energies. For simplicity we will not indicate explicitly this dependence in the following, but we will consider it in the analysis of our data.

The differential cross section is then obtained in terms of the generalized susceptibility $\chi(\beta,\omega,\mathbf{q})$ corresponding to the generalized density Eq. (2). It is related to the imaginary part $\chi''(\beta,\omega,\mathbf{q})$ of this susceptibility by

$$\frac{d^2\sigma}{d\Omega d\omega} = \frac{r_0^2}{\pi(1-e^{-\beta\omega})}\frac{\omega_S}{\omega_L}\chi''(\beta,\omega,\mathbf{q}), \tag{4}$$

where $r_0 = e^2/4\pi\epsilon_0 mc^2$. The standard procedure is then to calculate $\chi(\beta,\omega,\mathbf{q})$ in the superconducting state within the single bubble approximation. Moreover, it is appropriate to neglect the momentum transfer $\mathbf{q}$ because it is small compared to the inverse coherence length and almost perpendicular to the CuO_2 planes. One finds then within BCS theory and in the limit of low temperature $T \to 0$, which is relevant for our experiments,[3]

$$\chi''(\omega) = \frac{2\pi N_F}{\omega} \mathrm{Re} \left\langle \frac{|\gamma_{\mathbf{k}}|^2 \Delta_{\mathbf{k}}^2}{(\omega^2 - 4\Delta_{\mathbf{k}}^2)^{1/2}} \right\rangle. \tag{5}$$

N_F is the density of states for both spin orientations at the Fermi level and the brackets indicate an average over the Fermi surface. $\Delta_{\mathbf{k}}$ stands for the superconducting, $\mathbf{k}$-dependent gap. For our purpose, Eq. (5) has two related major drawbacks. First, it leads to a vanishing Raman scattering in the limit of large frequency, where we should recover the physical properties of the normal state. It also leads in general to a singular behavior in the vicinity of the thresholds for creation of a pair of excitations, which occurs at twice the maxima of the gap $\Delta_{\mathbf{k}}$. This is in contrast with our experimental results. As we will see, we obtain smooth spectral shapes, and, in the high-frequency regime, we recover a strong Raman scattering, which is well known in the normal state. These two discrepancies between experiment and theory can be ascribed to the fact that no collisional damping of any kind is included in the process of deriving Eq. (5). Nevertheless, this is not so important here since our purpose is much more to make a qualitative analysis of our results than to provide a full quantitative account of experiment. However, it is clear that inclusion of lifetime effects in the theory is quite desirable to provide a more accurate account of experimental results. Work in this direction is in progress and will be reported elsewhere.

Finally, there is a physical effect, essential for a proper analysis of Raman scattering, which we have not included up to now. Indeed, if we had a constant Raman vertex, we would merely look for a density-density response. As pointed out already by Wolff,[20,4] perfect screening in metals at long wavelength implies that, in this case, Raman scattering would be essentially zero. Therefore, it is necessary to include screening by the Coulomb interaction in order to obtain a proper physical result. In the limit of perfect screening, the result is

$$\chi''(\omega) = \mathrm{Re}\left[\chi_{\gamma\gamma}(\omega) - \frac{\chi_{\gamma 1}(\omega)\chi_{1\gamma}(\omega)}{\chi_{11}(\omega)} \right], \tag{6}$$

where $\chi_{\gamma\delta}$ is defined by

$$\chi_{\gamma\delta}(\omega) = \frac{2\pi N_F}{\omega} \left\langle \frac{\gamma_{\mathbf{k}} \delta_{\mathbf{k}}^{\star} \Delta_{\mathbf{k}}^2}{(\omega^2 - 4\Delta_{\mathbf{k}}^2)^{1/2}} \right\rangle. \tag{7}$$

Here $\gamma_{\mathbf{k}}$ and $\delta_{\mathbf{k}}$ are general vertices, 1 being the proper vertex for a true density interaction [this comes in Eq. (6) because only this true density is screened by Coulomb interaction]. In B_{1g} and B_{2g} symmetry, $\chi_{\gamma 1}$ is zero for symmetry reasons, the last term in Eq. (6) drops out and we merely recover Eq. (5). In other words, the B_{1g} and B_{2g} symmetry are not screened because the average effective density is zero in these cases. On the other hand, this is not so for the A_{1g} symmetry, and screening has to be properly taken into account by making use of Eq. (6). Nevertheless, one sees easily from this equation that any $\mathbf{k}$-independent contribution to the Raman vertex drops out of the result. Physically, such a contribution is irrelevant because it is fully screened out.

III. CRYSTAL CHARACTERIZATION

The measurements were carried on two single crystals labelled *A* and *B*. These crystals were grown by a single step synthesis as previously described for Hg-1223.[21] They are parallelepipeds with typical 0.5×0.5 mm^2 cross section and thickness 0.3 mm. The [100] crystallographic direction lies at 45° of the edge of the square and the [001] direction is normal to the surface. They were characterized by x-ray-diffraction and wavelength dispersive spectrometry.[22] Identification of the proper phase requires several experimental characterization techniques, and one may be easily mislead in particular by the critical temperature. The presence of intergrowth phases, corresponding to different stacking numbers of the CuO_2 planes along the *c* axis has been established.[22] This was detected through (i) the presence of diffusion streaks in the oscillation photographs, (ii) the lattice parameter values obtained from an Enraf-Nonius CAD-4 diffractometer at 293 K, (iii) the chemical analysis carried out using a Camebax SX50 electron probe. The electron beam probes 1 μm^3 of material at each measurement (the probed depth is approximatively 10 times the penetration depth of the excitation light). Twenty measurements were performed for the *A* crystal and 40 for the *B* crystal. The *A* crystal exhibits an overall composition of $Hg_{0.88}Ba_2Ca_{1.92}Cu_{2.88}O_{8+\delta}$. The understoechiometry in Ca and Cu can be assigned to the existence of Hg-1212 intergrowth phase. The *B* crystal has the following composition: $Hg_{0.96}Ba_2Ca_{2.26}Cu_{3.5}O_{8+\delta}$, which reveals a mixture of Hg-1223 and Hg-1234. A detailed x-ray analysis has been performed on the *A* crystal. The lattice parameters deduced from the diffractometer are $a = 3.844(2)$ Å and $c = 15.72(3)$ Å, hence the *c* parameter of this crystal is slightly smaller than the perfectly stoechiometric Hg-1223 ($c = 15.831$ Å) and definitely much larger than $c = 12.71$ Å for Hg-1212. Therefore, according to the composition and the lattice parameters and in agreement with the chemical probe, we may consider that we are dealing essentially with the Hg-1223 compound in both *A* and *B* crystals.

The crystals are slightly underdoped, with δ less than 0.1. δ refers to an excess of oxygen atoms randomly arranged within the Hg planes. Underdoping is further confirmed by dc magnetization measurements displayed in Fig. 1. Although there is an onset of diamagnetism around 133 K, it appears that the main transition occurs at $T_c \sim 126$ K. Resistivity values at T_c are similar to those of high quality YBCO single crystals with typically $\varrho(T_c) \sim (30-60)\mu\Omega$ cm.[23] Optimal doping increases δ, hence introduces disorder in the Hg basal plane. Therefore an underdoped system is closer to fourfold symmetry than an optimally doped one and is even more appropriate to symmetry considerations.

Finally, we wish to point out that the extensive study of the crystal structure described above had not been completed for all the samples (coming from a single batch) by the time

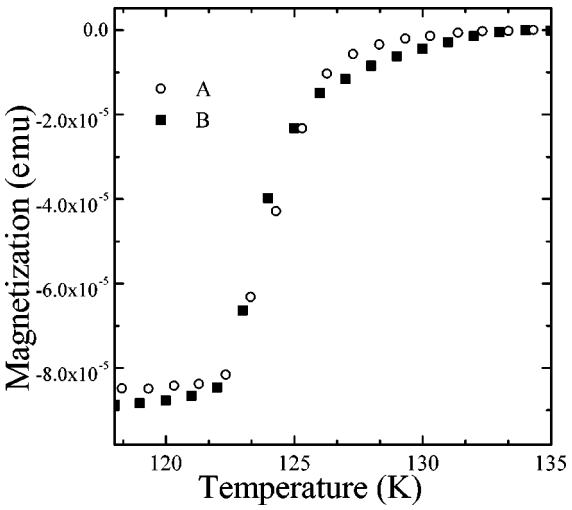

FIG. 1. dc magnetization recorded during field cooling in a 10 Oe field for *A* and *B* samples.

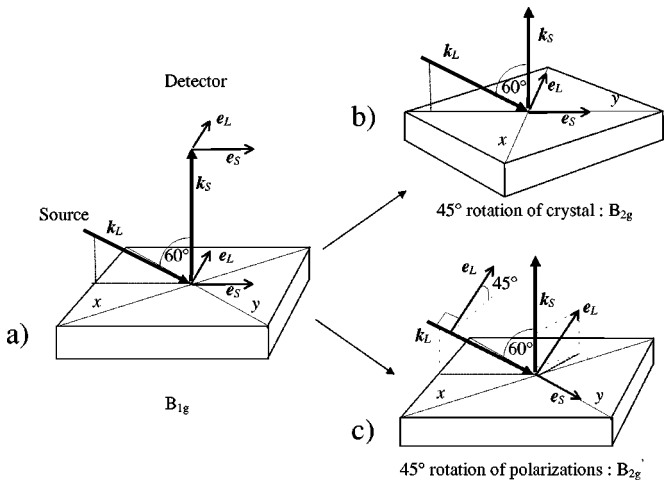

FIG. 2. Experimental configurations chosen to obtain the B_{1g}, B_{2g}, and B'_{2g} symmetries.

of our earlier work.[16] One crystal was clearly identified as Hg-1212, and we eventually published the better quality spectra from another one, unaware of the fact, which is established by now, that two crystals coming from the same batch may be either Hg-1212 or Hg-1223. The latter sample was subsequently analyzed and turned out to be, as explained above, Hg-1223. It is important to quote that actually the Raman spectra of the two samples studied in Ref. 16 were similar. This will be shown in the experimental results.

IV. EXPERIMENTAL PROCEDURE

Raman measurements were performed with a double monochromator using a single channel detection and the Ar^+ and Kr^+ laser lines. The spectral resolution was set at 3 cm^{-1}. The crystals were mounted in vacuum (10^{-5} mbar) on the cold finger of a liquid-helium flow cryostat. The temperature was controlled by a Si diode located inside the cold finger. The incident laser spot is less than 100 μm in diameter and the intensity onto the crystal surface was kept below 50 W cm^{-2} in order to avoid heating. At our lowest temperature, the difference in temperature between the cooled face and the illuminated face of the crystals was estimated to be $\sim$1 K, resulting in a temperature of 13 K inside the scattering volume, instead of a nominal 12 K temperature. The incidence angle was 60°. The scattered light was collected along the normal to the crystal surface. The polarization is denoted in the usual way: $x[100]$ (a axis), $y[010]$, $z[001]$ (c axis), $x'[110]$, $y'[1\bar{1}0]$. In order to compare our experimental data with the theoretical calculations,[6,22] the pure B_{2g} (xy) and B_{1g} $(x'y')$ symmetries are convenient and well suited for the investigation of a $d_{x^2-y^2}$ order parameter. To make this point clear, we recall briefly the symmetry properties: in the B_{1g} case, the Raman vertex $\gamma_{\mathbf{k}}$ is zero by symmetry for $k_x=k_y$, so the electronic scattering is insensitive to the gap structure around 45°; in contrast, the $k_x=0$ and $k_y=0$ regions do contribute, giving weight to the gap Δ_0 in these directions. Conversely, in the B_{2g} case, the Raman vertex $\gamma_{\mathbf{k}}$ is zero by symmetry for $k_x=0$ or $k_y=0$ or and nonzero elsewhere, hence provides weight in the $k_x=k_y$ direction.

In our experimental procedure, we start by measuring the B_{1g} channel. The incident angle being not zero, the crystal is then rotated by 45° in order to get the B_{2g} one, the polarizer and the analyzer remaining unchanged [see Figs. 2(a) and 2(b)]. The $A_{1g}+B_{1g}$ and $A_{1g}+B_{2g}$ symmetries are obtained from the (xx) and $(x'x')$ polarizations, respectively. Any contamination of the $A_{1g}+B_{2g}$ channel by the B_{1g} channel through polarization leakage is ruled out: indeed, in the former configuration, we have removed the half wavelength plate that must be inserted between the analyzer and the entrance slit of the spectrometer when we want to detect the B_{1g} channel. The reason is that the grating reflection factor depends strongly on the incoming polarization; in the $A_{1g}+B_{2g}$ channel, the polarization of the scattered light is the one which is favored by the grating, in contrast with the B_{1g} channel where the polarization of the scattered light is crossed relative to the former case.

In order to probe the same area for all symmetries, the impact of the laser beam onto the crystal surface was precisely located before turning the crystal. Finally, a very weak diffusive spot was carefully selected on each crystal in order to minimize the amount of spurious elastic scattering. Another possibility that guarantees that the location of the laser spot is unchanged for B_{1g} and B_{2g} symmetries, is to rotate the polarization instead of the crystal [see Fig. 2(c)], when starting from pure B_{1g} symmetry. After a 45° rotation, the incident electric field no longer lies within the xy plane, which induces symmetry mixing for B_{2g}. We have estimated the amount of mixing with $A_{1g}+B_{1g}(xx)$ and $E_g(xz)$, taking into account the high refractive index ($\sim$2), which brings the propagation of the beam inside the crystal closer to normal incidence; we found $\sim$5% admixture of $A_{1g}+B_{1g}(xx)$ and $\sim$16% of $E_g(xz)$. We shall denote this mixed symmetry as B'_{2g}. Similarly, we can measure the A'_{1g} channel (bringing the analyzer parallel to the polarizer), which comprises besides the $A_{1g}+B_{1g}$ spectrum, $\sim$5% of $B_{2g}(xy)$ and $\sim$16% of $E_g(xz)$.

To get a complete set of reliable data, we have performed Raman measurements in both configurations: (i) rotation of the crystal without changing the polarization, so as to get pure B_{1g} and B_{2g} symmetries and (ii) rotation of the polarization without moving the crystal, in order to work with the

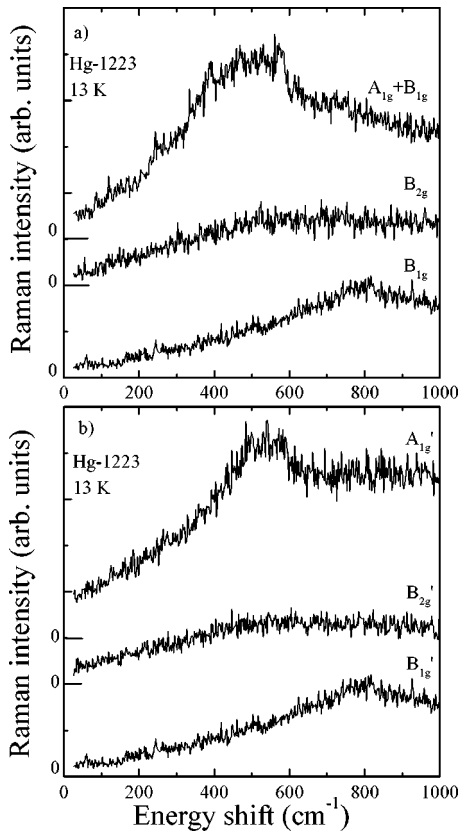

FIG. 3. Raw Raman spectra of the Hg-1223 (sample A) at $T=13$ K obtained from both configuration described in Fig. 2. (a) $A_{1g}+B_{1g}$, pure B_{2g} and B_{1g} symmetries (obtained by rotating the crystal). (b) mixed A'_{1g} and B'_{2g} symmetries (obtained by rotating the polarization).

same spot. Various spots have been probed on each crystal. All the resulting data are consistent one with the other.

V. EXPERIMENTAL RESULTS

The Hg-1223 raw spectra at 13 K, in the three symmetries obtained with the 514.52 nm laser line by rotating the crystal are displayed in Fig. 3(a). These pure $A_{1g}+B_{1g}$, B_{1g}, and B_{2g} spectra were previously reported in Ref. 16. Figure 3(b) shows the spectra obtained by rotating the polarization, yielding the A'_{1g} and B'_{2g} mixed symmetries. The two procedures (performed in the same A crystal) yield similar results for each symmetry, although there is some extra scattered intensity in the mixed A'_{1g} symmetry at high energy. Since several spots have been selected, this crossed procedure confirms the reliability of the data. Note that due to the high surface quality of the Hg-1223 crystal, the residual elastic scattering is confined below 50 cm^{-1} and is quite weak. In crossed polarization measurements (B_{1g} and B_{2g}), this scattering is just not seen, hence no correction has been performed to take it into account. The $A_{1g}+B_{2g}$ spectrum obtained from the B crystal is displayed in Fig. 4. For the sake of the comparison, we show in Fig. 5 preliminary raw spectra from Hg-1212. The surface quality being not so good for this sample, we see clearly, especially in the A_{1g} symmetry, the Rayleigh scattering. Nevertheless, these results are suggestive of a very strong similarity to the Raman response in both compounds.

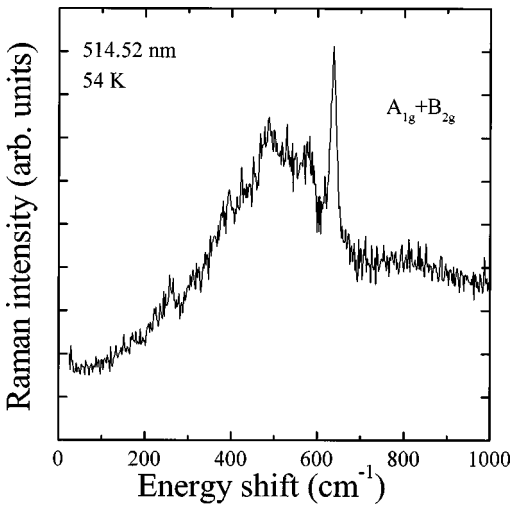

FIG. 4. Raw Raman spectrum of Hg-1223 (sample B) at $T=54$ K in $A_{1g}+B_{2g}$ symmetry. Note the shoulder that develops on the high energy side at 800 cm^{-1}.

A. The electronic maxima

Let us focus on Figs. 3 and 4. Remarkably, and in sharp contrast with Y-123 and Bi-2212, we get a large spectral range below the energy gap where no Raman active phonon mode hinders the B_{1g} and B_{2g} electronic scattering analysis. Weak and narrow peaks appear at 240, 388, 480, and 580 cm^{-1} in the $A_{1g}+B_{1g}$ and $A_{1g}+B_{2g}$, but their energy location and their intensity are such that no correction is actually needed to discuss the electronic spectra. The 580 cm^{-1} peak shows a phonon asymmetric line shape with an antiresonance on the high-energy side [see Fig. 3(a)]. This is characteristic of the interference between an electronic continuum and a single phonon state. This Fano line shape has already been detected in Y-123 and Bi-2212 for the B_{1g} normal mode in the vicinity of the gap structure maximum.[7,10,24] The 640 cm^{-1} peak detected in Fig. 4 is assigned to some trace of $BaCuO_2$ impurity.[25] Overall, the spectra do not require the delicate handling of ''phonon subtraction'' and we are in a position to turn immediately to the analysis of the data.

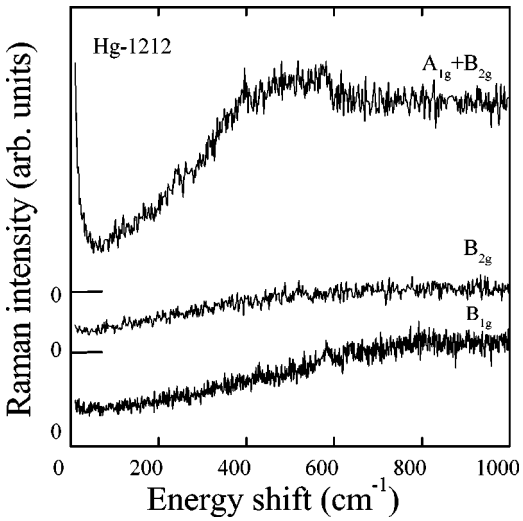

FIG. 5. Raw Raman spectra of Hg-1212 taken at 13 K (shown for comparison with Fig. 3).

TABLE I. Overview of the energy location of the two electronic maxima observed by Raman spectroscopy in various cuprates near the optimally doped regime.

	Y-123[a]	Bi-2212[b]	LaSr(x)-214[c]	Tl-2201[d]	Hg-1223
Stoichiometry	6.95	(See Ref.)	$x=0.17$	(See Ref.)	See Sec. III
T_c (K)	90	86	37	80	127
ω_l (cm^{-1})	340	350	125	300	540
ω_h (cm^{-1})	550	500	200	450	800
$\hbar\omega_l/k_BT_c$	5.6	6.1	5.1	5.6	6.4
$\hbar\omega_h/k_BT_c$	9.1	8.7	8.1	8.4	9.4
ω_h/ω_l	1.6	1.4	1.6	1.5	1.5

[a]Reference 7.
[b]Reference 9.
[c]Reference 12.
[d]Reference 11.

Two well-marked maxima are observed: one is located around 530 cm^{-1} in the $A_{1g}+B_{1g}$ [Fig. 3(a)], $A_{1g}+B_{2g}$ (Fig. 4) symmetries and the A'_{1g} [Fig. 3(b)] mixed symmetry; the other is observed at 800 cm^{-1} in the B_{1g} symmetry. In contrast, no clear maximum appears in the B_{2g} and the mixed B'_{2g} symmetries, for which actually the scattered intensity levels out smoothly around 530 cm^{-1}.

In the $A_{1g}+B_{1g}$ spectrum [Fig. 3(a)], we observe a weak shoulder near 800 cm^{-1}, not seen in the mixed A'_{1g} symmetry [Fig. 3(b)]. In the $A_{1g}+B_{2g}$ spectrum (Fig. 4), beyond the well-defined maximum at 530 cm^{-1}, a broad maximum is clearly visible at 800 cm^{-1}. There is, in the latter case, no possible contamination by the B_{1g} channel (see Sec. IV), whereas the B_{2g} channel does not display any feature above 500 cm^{-1}. All this strongly suggests that the 800 cm^{-1} maximum is an intrinsic electronic feature in the A_{1g} channel. This important point will be discussed later.

The observation of two electronic maxima below T_c is currently mentioned for two distinct channels.[7–9,13] It is a common feature for numerous high-T_c cuprates studied by Raman spectroscopy near the optimally doped regime. The lower-energy peak ω_l is usually observed in $A_{1g}+B_{1g}$ symmetries and the higher-energy one ω_h is detected in pure B_{1g} symmetry. The energies of these two peaks for various cuprates are listed in Table I. Two well-defined energy scales appear: $(5-6.4)k_BT_c$ and $(8-9.4)k_BT_c$. Remarkably enough, their ratio is approximatively 1.5, whatever the compound. What is new in our study is that, by looking at a less commonly studied symmetry channel, we find that these two energy scales are present within one single channel, namely, A_{1g}.

Finally, the temperature dependence of the imaginary parts of the electronic response for the $A_{1g}+B_{2g}$ and B_{1g} symmetry as a function of the temperature from 13 to 150 K is shown in Fig. 6(a) and 6(b), respectively. The imaginary part of the electronic response function Im $\chi[\omega,T]$ is derived by subtracting the photomultiplier dark current, the Rayleigh scattering intensity, when present, and by correcting for the response of the diffraction grating and for the Bose-Einstein factor $n(\omega,T)=[\exp(\hbar\omega/kT)-1]^{-1}$. In both symmetries, the low-energy scattered intensity increases, approaching that of the normal state as the temperature is raised. The maxima at 540 cm^{-1} (for $A_{1g}+B_{2g}$) and 800 cm^{-1} (for B_{1g}) gradually collapse and disappear above T_c. These two maxima do not shift significantly (at most 10%) towards low energies as the temperature increases. The latter result is fairly general in Raman and tunneling experiments.

B. The low lying energy excitations

We wish now to concentrate on the low-energy part of the spectra. We collect in Fig. 7 the imaginary parts of the electronic response functions Im $\chi[\omega,13\text{ K}]$ obtained from the raw data after performing the same corrections described just above, associated to the $A_{1g}+B_{1g}$, B_{1g} and B_{2g} symmetries, already reported in Ref. 16. The dotted lines represent

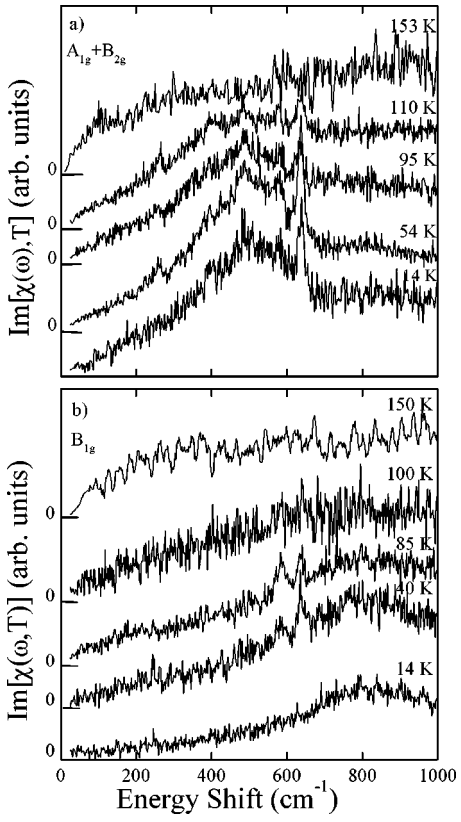

FIG. 6. Imaginary part of the response functions at various temperatures (sample *B*) (a) $A_{1g}+B_{2g}$ spectrum. (b) B_{1g} spectrum.

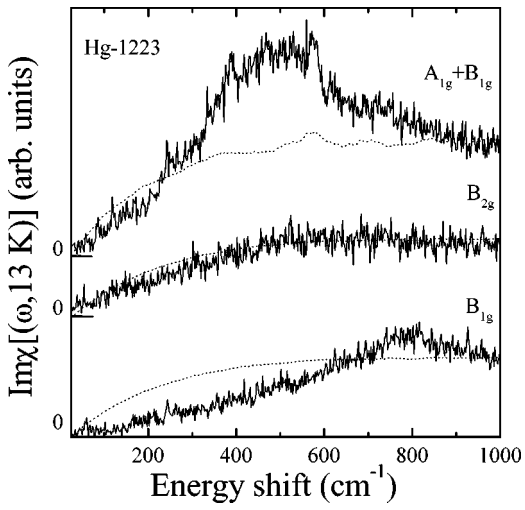

FIG. 7. Imaginary parts of the response function Im[$\chi(\omega,T=13\ \mathrm{K})$] deduced from experimental data of Fig. 3. The dashed lines represent Im[$\chi(\omega,T=150\ \mathrm{K})$].

Im χ[ω,150 K], after smoothing the spectra (for clarity). As could be inferred from the raw spectra, the three response functions seem to extrapolate to zero at zero frequency, within our experimental accuracy. We recall[16] the main observations that emerge from Fig. 7, namely,

(i) the B_{1g} response function exhibits a clear decrease of the electronic scattering at low energy in the superconducting state with respect to the normal state. In contrast, the $A_{1g}+B_{1g}$ and B_{2g} response functions decrease barely at low energy. Actually, there is very little change between the normal and the superconducting state in the B_{2g} channel. The change is instead much larger in the A_{1g} channel but occurs around the peak energy.

(ii) the B_{1g} spectrum exhibits a steady quasilinear increase with energy, in contrast with Bi-2212 spectra where, after subtracting the phonon contribution, the spectrum below the peak energy exhibits a strong upward curvature.[6]

(iii) the electronic response functions in the normal and superconducting state merge in all three symmetries around 1000 cm^{-1}.

To investigate further the low-energy behavior of the B_{1g} spectrum in the superconducting state, we have performed Raman measurements at $T=13$ K with various excitations lines. The imaginary parts of the electronic response functions in the B_{1g} symmetry are displayed in Fig. 8(a) for five different excitation lines, namely, 647.1, 568.2, 514.52, 488.0, and 476.5 nm. For clarity, the spectra have been normalized so as to achieve the same intensity around the 800 cm^{-1} maximum and shifted vertically. The spectra reported here have been taken from sample B. There is a clear change in the overall shape of electronic response as the excitation energy decreases.

A simple visual inspection of the spectra suggests that they can be classified in two categories: for the 647.1 and 568.2 nm lines, the linear part appears to extend up to higher energy than for the 514.52, 488.0, and 476.5 nm excitation lines. Also the maximum for the two former ones seems to develop at a somewhat lower energy. In order to confirm the occurrence of two sets of data displaying a similar spectral dependence, we have firstly checked quantitatively that

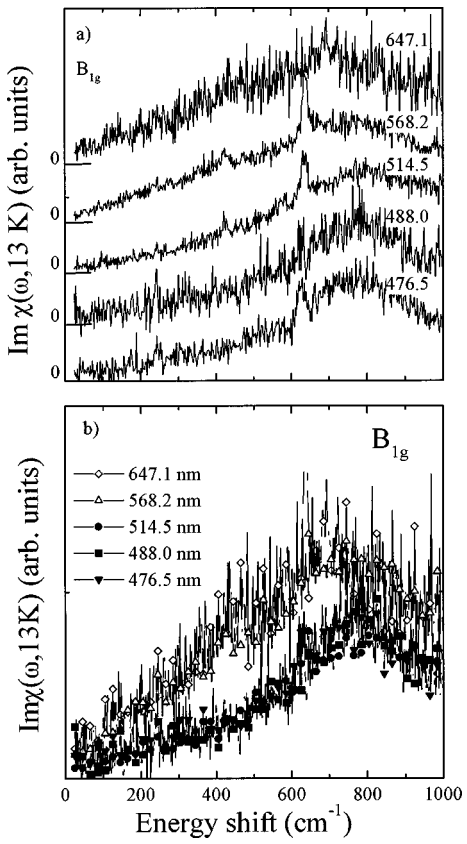

FIG. 8. Imaginary part of the response function Im[$\chi(\omega,T=13\ \mathrm{K})$] in B_{1g} symmetry, obtained from various excitation laser lines (sample B). Zero amplitude is indicated by the short solid line. (a) after normalization of the amplitude at the peak energy. (b) a different normalization (see text) shows that the data can be gathered into two sets of spectra displaying the same frequency dependence.

within the two sets, the spectra are indeed proportional. Then, we have used this calculation to normalize the spectra for the two lower-energy excitation lines (647.1 and 568.2 nm) on one hand, and for the three higher-energy excitation lines (514.52, 488.0, and 476.5 nm) on the other hand. The result is shown in Fig. 8(b). Indeed, within each set, the higher excitation energy spectra and the lower ones fall exactly one on top of the other, within our experimental resolution.

As mentioned in Sec. II, a source of complication of the analysis may arise from the dependence of the Raman vertex on ω_L and ω_S. The dependence on ω_L is revealed in our experiments as a change in the strength of the Raman scattering with the laser frequency. The dependence on ω_S translates into a dependence on the Raman shift $\omega=\omega_L-\omega_S$, which could affect the validity of the low-frequency analysis.

Let us first comment on the possible origin of the ω_L dependence. It is interesting to note that in the spectral range of interest (15 000–22 000 cm^{-1}), various cuprates (YBCO, LaSrCuO, BiSrYCuO) exhibit two bands, located typically around 12 000–14 000 cm^{-1} (the so-called charge-transfer band), and 22 000 cm^{-1}.[26–29] Since, to the best of our knowledge, similar spectra are not yet available for the Hg compounds, we assume that the absorption bands lie in the same range as for other cuprates. The three high-energy ex-

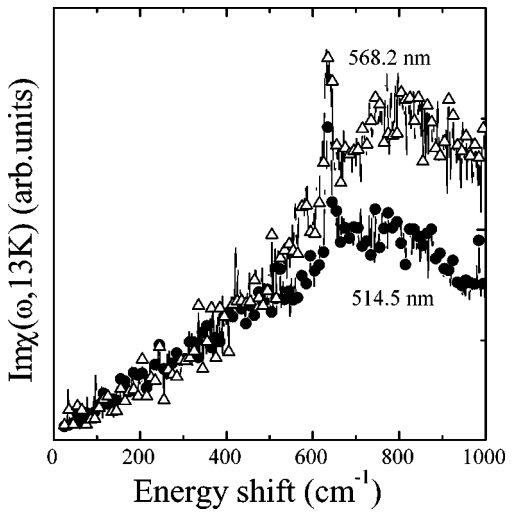

FIG. 9. Imaginary part of the electronic response for two excitation lines (514.5 nm, circles, and 568.2 nm, triangles) previously shown in Fig. 8(b) as belonging to the two sets of data. Within a scale factor, it appears clearly in this plot that the low-frequency response exhibits the same frequency dependence up to 500 cm^{-1} for both excitation lines.

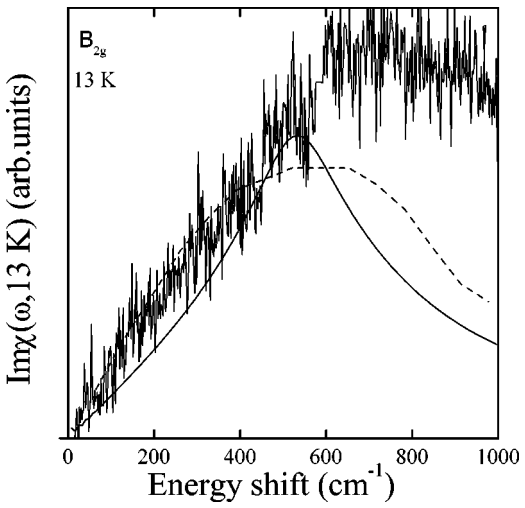

FIG. 10. B_{2g} data (sample *A*) and calculations for the $d_{x^2-y^2}$ model (dashed line) and for a model with 8 nodes lying at $\theta_0=26^0$ (solid line).

citation lines are clearly located in the absorption range of the high-energy band. The 568.2 nm line (17 600 cm^{-1}) actually lies inbetween the two bands, still closer to the charge transfer band, and the Raman spectrum exhibits a strong similarity with the 647.1 nm (15450 cm^{-1}) one. The latter is definitely in the vicinity of the charge-transfer band. Therefore, the change of the Raman spectra with the excitation energy bears an actual consistency with the absorption bands in the visible range, supporting the idea that resonant scattering is effective. It is not very surprising that we find within our experimental resolution, that the data can be separated into two sets, since two bands seem to be involved. The question that is raised once this is recognized is which frequency range is most affected by the change of the Raman vertex with energy. When fitting the absorption bands to Lorentz oscillators,[26] we found typical widths of 1 eV. A typical energy scale for the variation of the Raman vertex with ω would then be 0.5–1eV.

A first-order expansion of the Raman vertex (we omit the **k** dependence of γ_k for simplicity) with respect to the laser frequency writes

$$\gamma(\omega_L,\omega)=\gamma(\omega_L,0)+\omega\left(\frac{\partial\gamma(\omega_L,\omega)}{\partial\omega}\right)_{\omega=0}. \qquad (8)$$

Therefore, in the limit $\omega\rightarrow 0$, which is of interest here, the Raman vertex is independent of ω, which implies that the low-frequency behavior should not depend on the laser excitation energy. As ω increases, the frequency dependence of γ may not be neglected. Using this line of reasoning, we have compared the low-frequency dependence of the two sets of spectra obtained by varying the laser excitation. A simple way to do it is to select from each set the spectrum exhibiting the best signal to noise ratio, namely the ones associated to the 568.2 and the 514.5 nm lines. Figure 9 shows that indeed, the low frequency dependence (up to 500 cm^{-1}) is the same, and that the spectra gradually separate as the frequency increases. We assign this behavior to the change of the Raman vertex with frequency, as explained above. Therefore, we shall consider henceforward that there is no change of the low-frequency behavior when changing the excitation energy. Note incidentally the strong linear term of the B_{1g} spectrum, best seen in Fig. 9.

VI. DISCUSSION

We may now turn to the comparison of our data with existing theories. We start with the $d_{x^2-y^2}$ model, as computed by Devereaux, which was found to describe well the Bi-2212 results.[30] In a pure $d_{x^2-y^2}$ model, symmetry considerations imply that the B_{1g} spectrum is insensitive to the nodes at 45° (hence the ω^3 dependence) and displays a maximum at $2\Delta_0$, whereas the B_{2g} symmetry exhibits a linear low-frequency dependence (because it probes the nodes) and a smeared gap.[16] For the same reason the A_{1g} symmetry has also a linear low ω behavior. We find a fair agreement of this model with our data for the linear dependence of the low-energy part of the B_{2g} symmetry (see Fig. 10).

Our linear A_{1g} spectrum agrees also quite well with the prediction of the $d_{x^2-y^2}$ model at low frequency, but this is not the case for the higher frequency range [Fig. 12(a)]. Indeed, we note that the $d_{x^2-y^2}$ model has only a single maximum that gives rise to a single peak, both in B_{1g} and A_{1g} symmetry. Naively, one expects these two peaks to be essentially at the same frequency. This is already in contrast with experiments on Bi-2212 where the A_{1g} peak is found at much lower frequency than the B_{1g} one. Nevertheless, if one takes into account the strong screening in the A_{1g} symmetry together with a sizeable smearing, one may obtain a large softening of the A_{1g} peak and reconcile theory with experiment. However, we find it eventually difficult in our calculations to get the necessary softening without obtaining simultaneously an unduly wide maximum. We give an example of such a calculation in Fig. 12(a). Anyway, our present observation of two distinct peaks in the same A_{1g} channel deduced from the $A_{1g}+B_{2g}$ symmetry (see Fig. 4) cannot be reconciled with a pure $d_{x^2-y^2}$ model. We note that

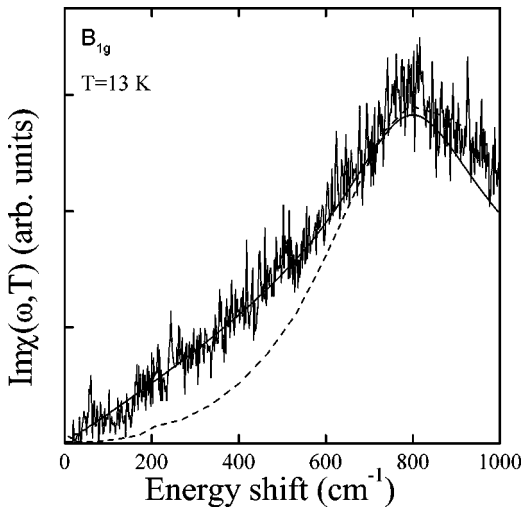

FIG. 11. B_{1g} data (sample A) and calculation for the $d_{x^2-y^2}$ model (dashed line) and for a model with 8 nodes lying at $\theta_0 = 26^0$ (solid line).

the second peak, essentially at the same frequency as the B_{1g} one, had not been seen in our earlier experiments[16] because only the $A_{1g}+B_{1g}$ symmetry had been measured.

Finally, we consider the B_{1g} symmetry which, together with the B_{2g} symmetry, is easier to analyze because it is not affected by screening, in contrast with the A_{1g} symmetry. Most strikingly, the low-frequency behavior of the theoretical $d_{x^2-y^2}$ B_{1g} spectrum is incompatible with our experimental results. In the $d_{x^2-y^2}$ model, the response function for B_{1g} should increase as ω^3 (Ref. 6) and it is clear, by inspection of Fig. 9 and 11, that our results are essentially linear in frequency. If we analyze our data more quantitatively, we have to recall that such a power-law behavior is an appropriate description only at low frequency, and therefore the pending question is the choice of the proper energy scale when trying to fit the results. Fitting the spectrum from Fig. 11 to a power law ω^α, up to 300 cm^{-1} yields $\alpha = 1.5 \pm 0.5$ inconsistent with an ω^3 dependence.[16] However, the choice of the energy range for fitting may be disputable, and a second fit to $b\omega + c\omega^3$ was attempted in order to provide a more accurate estimate of the relative weight W of the linear part with respect to the cubic part. W was computed over various energy ranges, e.g., up to 300, 400, 500, and 600 cm^{-1}, still using the spectra shown in Fig. 11. Actually, referring to Fig. 9, the low-energy range of interest may not exceed 500 cm^{-1}. We found $W = 2 \pm 1$, 4 ± 1, 3.3 ± 0.7, 3.4 ± 0.5, meaning that a dominant linear component must be taken into account, inconsistent with a pure $d_{x^2-y^2}$ model. B_{1g} being linear at low frequency appears to agree with the Tl-2201 results, at least at high enough excitation energy ($\hbar\omega > 2.18$ eV, or $\lambda < 5734$ Å).[31]

It has been argued that impurities are responsible for the observed low-frequency density of states in the B_{1g} channel. Devereaux[32] has indeed shown that, in the unitary limit, for a $d_{x^2-y^2}$ gap, impurities induce for B_{1g} a linear rise of the electronic scattering at low frequency, crossing over to the ω^3 dependence at higher frequency. The crossover energy ω^* found in this case is typically the width γ of the band of states bound to impurities.[33] For unitary scatterers this width is of order $\gamma \sim (\Gamma\Delta_0)^{1/2}$ where $\Gamma = n_i/(\pi N_F)$ with n_i the impurity concentration and Δ_0 the maximum of the d-wave gap. In the Born limit it is, in general, much smaller, $\gamma \sim 4\Delta_0 \exp(-\pi\tau\Delta_0)$, where τ is the normal-state relaxation time, and impurities bring no qualitative change in the density of states at low energy[33] except for large relaxation rates. Therefore, the unitary case is the most favorable one for an important effect of impurities on Raman scattering. However, this is a very specific case, and experimental support is still lacking. Note that in the case of a small or intermediate relaxation rate, one goes rapidly out of the unitary regime as soon as the scattering phase shift goes away from $\pi/2$. Only for a large relaxation rate $1/(2\tau\Delta_0) > 0.3$ does the unitary regime extend over a fair range of scattering phase shifts. In the absence of experimental evidence, a random distribution of scattering phase shifts would seem a reasonable assumption.

It is worth recalling that this assumption of unitary scatterers was raised[33,34] in order to reconcile the robustness of the critical temperature against impurity scattering, which is unexpected in a d-wave superconductor, with the much less robust temperature dependence of the London penetration depth, whose linearity is thought to be affected by scattering. Nevertheless, due to the difficulty of measuring the absolute value of the penetration depth, there is no strong experimental evidence for this assumption. Actually, published data are somewhat contradictory.[35–37] Let us nevertheless consider this unitary limit. Our experimental results can be compared reasonably well with Devereaux's calculation,[32] taking $\Gamma \sim 0.5\Delta_0$. This means a scattering rate Γ of order of the gap Δ_0 itself. Such a high scattering rate should strongly reduce the critical temperature or even destroy completely superconductivity. This is in marked contradiction with $T_c = 126$ K of our single crystals that does not differ in an appreciable way from the critical temperature of supposedly rather clean crystals. It is also in contradiction with the main value of $\rho(T_c)$ (see above in Sec. III). For example $\Gamma \sim 200$ cm^{-1} could yield $\rho(T_c)$ larger than typically 100 $\mu\Omega$ cm. Finally, we remark that the fairly sharp structure that we observe in A_{1g} is difficult to reconcile with a large scattering rate. Altogether this makes rather unlikely the explanation of the linear behavior of the low frequency B_{1g} by an impurity effect.

Accordingly, we consider that our results are representative of pure crystals. Then an inescapable consequence of the observed linear frequency dependence is the occurrence of a finite density of states exhibiting a similar energy dependence, which is most naturally assigned to nodes in the gap. Since these nodes are probed in both B_{1g} and B_{2g} symmetries, they cannot be located only in the 45° direction. We are thus left with the conclusion that nodes exist outside the 45° direction. It is worth recalling that although Raman scattering probes the electronic excitations along various **k** directions, it cannot give accurately the location of the nodes.[16] We have therefore to explore this point more quantitatively.

From the low-energy part of our spectra, we know there are nodes outside the 45° direction. It can readily be seen that a small shift of the nodes away from 45° is not enough to account for experiment. Indeed, if we use a toy model $\Delta(\theta) = \Delta_0 \cos(2\theta - 2\alpha)$ obtained by artificially rotating the $d_{x^2-y^2}$ order parameter by an angle α, we find that a rotation by $\alpha \approx 10^0$ is barely noticeable in the spectra: the linear rise at low ω produced in B_{1g} by this rotation is quite small and

the spectrum is essentially unchanged within experimental accuracy.

Having at this stage exhausted all information contained in the low-energy dependence, in order to build up a specific model more appropriate than $d_{x^2-y^2}$, we have to rely now on the high-energy part of our spectra. While the B_{2g} symmetry offers only a hint of a maximum around 500 cm^{-1}, the B_{1g} symmetry and the A_{1g} symmetry are much more informative. Indeed, we have the occurrence of two maxima at 500 and 800 cm^{-1}, seen simultaneously in pure A_{1g} symmetry. The last one is seen separately in B_{1g} in a very clear way while the former is compatible with the structure seen in the B_{2g} symmetry. Together these observations strongly suggest two different energy amplitudes for the gap.

We assume that the gap has the symmetry of one of the one-dimensional representation of the tetragonal group, namely, A_{1g}, B_{1g}, B_{2g}, or A_{2g}. We need only to consider the range of the Fermi surface where the wave vector **k** has an angle θ with the x axis between 0 and $\pi/4$. The rest can be deduced by symmetry operations. Our model must accommodate a main maximum M, a secondary maximum M'—for the absolute value of the order parameter—and at least one node N (we assume for simplicity that there is only a single secondary maximum and no secondary minimum since there is no experimental evidence for them). This does not match with any of the simplest representative for the order parameter, namely, $k_x^2+k_y^2$ (A_{1g} symmetry), $(k_x^2-k_y^2)$ (B_{1g} symmetry), $k_x\,k_y$ (B_{2g} symmetry), or $k_x\,k_y(k_x^2-k_y^2)$ (A_{2g} symmetry). For instance, as pointed out by Leggett, the simple A_{2g} symmetry is compatible with the low-energy part of our spectra; but it does not provide a proper account of the high-energy part since it would give only peaks at a single frequency corresponding to the maximum of the gap. Therefore, we have to deal with a more complicated order parameter. From symmetry we must find at 0^0 either M or M' or N, and similarly at 45° (we eliminate the possibility of a discontinuous order parameter). Since the main maximum M is seen in B_{1g} symmetry and not in B_{2g} symmetry, we have to put it at 0°. Similarly, the secondary maximum M' being inferred in B_{2g} symmetry but not seen in B_{1g} symmetry implies a location at 45°. Then the only place left for nodes is somewhere between 0° and 45°. Since we have assumed a single secondary maximum, we can put only one node there. This leads to an order parameter that has over the whole Fermi surface 4 (equivalent) M, 4 M' and 8 nodes. Since this order parameter is continuous and is nonzero at 0° and 45° it has the A_{1g} symmetry. Therefore, we come to the conclusion that our Raman-scattering data imply an order parameter that does not break spontaneously the crystal tetragonal symmetry. However, it is clear that any slight shift of M and M' away from their symmetric locations will essentially not be felt in the resulting spectra. For example since our B_{2g} is quite featureless, we may worry that the presence of the main maximum M is washed out in it. So M could be away from 0°. Since M' is at 45° we can only put a node at 0°. But there is a node away from 0° because B_{2g} is linear at low frequency. The only location for this node is between M and 45° We end up with an order parameter which has the B_{2g} (d_{xy}) symmetry, with 8 M, 4 M' and 12 nodes over the whole Fermi surface. Similarly, we might worry that a small contribution of M' to the B_{1g} spectrum is not seen in our experimental results. However this seems almost incompatible with our data, except if M' is quite near 45°, but this would lead to an almost discontinuous order parameter since we have to put a node at 45°. In this way we would have a B_{1g} symmetry order parameter, with 4 M, 8 M' and 12 nodes on the Fermi surface. Finally, we could also think of putting nodes at 0° and 45° with M and M' slightly away from these locations. We would need to put a node between them. Hence, we would have a A_{2g} order parameter, with 8 M, 8 M', and 16 nodes. Again this is hardly compatible with our B_{1g} data. In conclusion the A_{1g} order parameter is at the same time the simplest and the most compatible with our data. In the following we will concentrate on this symmetry and investigate it more quantitatively.

A simple one-parameter model having the A_{1g} symmetry and satisfying the above requirements is $\Delta(\theta)=\Delta_0[\cos(4\theta)+s]$ where $s=(\Delta_M-\Delta_m)/(\Delta_{M+}\Delta_m)$ and $\Delta_0=(\Delta_M+\Delta_m)/2$. The gap maximum Δ_M is obtained for $\theta=0$ while the secondary maximum Δ_m occurs for $\theta=\pi/4$. The node lies at $\theta_0=(1/4)\arccos(-s)$ and in this simple model its location is linked to the ratio Δ_m/Δ_M. Naturally, by introducing other parameters we can decouple these two quantities, as we will consider briefly below. Since we make the choice $s=0.27$ according to experiment, we find obviously the peaks for B_{1g} and B_{2g} in agreement with our experimental results (Figs. 10 and 11). We calculate the Raman spectra for B_{1g} and B_{2g} symmetry by taking for the Raman vertices the simplest form compatible with symmetry, namely, $\gamma_{B_{1g}}\sim\cos 2\theta$, $\gamma_{B_{2g}}\sim\sin 2\theta$ and a density of states independent of θ. Naturally, the bare result for these spectra display a logarithmic singularity at their respective maximum and we have to invoke some broadening, most likely due to lifetime effects, in order to obtain theoretical results compatible with experiment. In this paper we include this broadening at the most phenomenological level by merely convoluting the bare result with a broadening function. We take a simple normalized Lorentzian for this function. However, we expect lifetime effects to be quite small at low energy and to grow progressively at higher energy. We account for this by choosing the width $\Gamma(\omega)$ of our Lorentzian proportional to the frequency at which we are looking: $\Gamma(\omega)=a\omega$. Explicitly, our final spectrum $F(\omega)$ is obtained from the bare spectrum $B(\omega)$ by $F(\omega)=\int d\omega'\,L(\omega-\omega',\omega)B(\omega')$ where $L(\omega-\omega',\omega)=(1/\pi)\Gamma(\omega)/[(\omega-\omega')^2+\Gamma^2(\omega)]$. Here the integration goes from $-\infty$ to $+\infty$ and $B(\omega)$ is extended by symmetry $B(-\omega)=-B(\omega)$ in the whole frequency range. This broadening method insures $F(0)=0$, whatever $\Gamma(\omega)$. In Figs. 10 and 11 we have taken our broadening parameter $a=0.15$. Note that this parameter is our only way to adjust the peak height with respect to the low-energy part of the spectrum. Hence, the fact that we find a good agreement in B_{1g} with experiment with a reasonably small broadening is satisfactory (Fig. 11). This is directly due to the fact that our node location $\theta_0=26°$ is far enough from 45°, otherwise we would have trouble obtaining a strong enough low-energy spectrum for B_{1g}, as we have seen in our toy model. As expected, the part of the experimental spectrum above the peak frequency is not properly described by our model, inasmuch as we go toward higher energy. This is merely due to

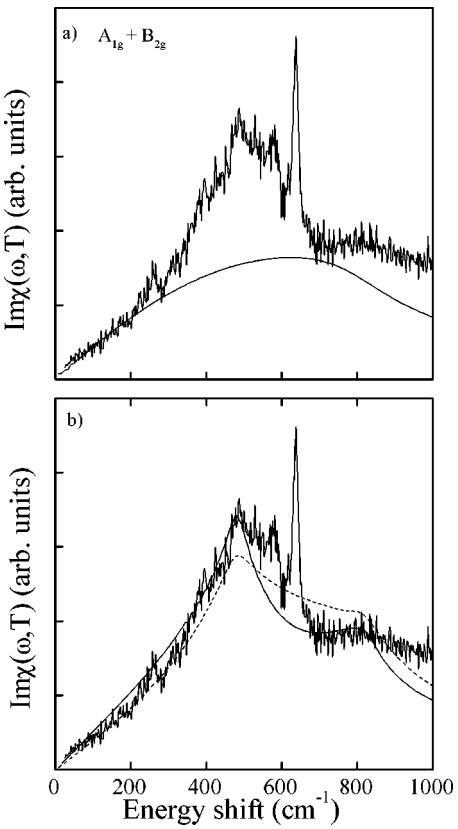

FIG. 12. $A_{1g}+B_{2g}$ spectrum (sample B) and calculations (a) for the $d_{x^2-y^2}$ model (solid line). (b) $s=0.27, A=0.05, a=0.03$ (solid line), $S=3.6$, $\theta_0=35^0$, $a=0.05$ (dashed line).

the fact that our theoretical result goes to zero for very high energies, in contrast with experiment. This discrepancy would be cured, at least partially, by taking proper account of lifetime effects, but this is beyond the scope of the present paper. In particular, we ascribe the moderate agreement between theory and experiment in B_{2g} symmetry to strong lifetime effects in this channel (Fig. 10).

We consider now in detail the A_{1g} symmetry. In our theoretical analysis, we take screening fully into account in the standard way. This feature makes the interpretation of the A_{1g} spectrum less easy than the B_{1g} or B_{2g} spectrum, because the result is not systematically related in an intuitive way to the shape $\Delta(\theta)$ of the order parameter. The most obvious manifestation of this is the fact that a constant A_{1g} Raman vertex gives a zero contribution because of full screening. Therefore, we have to look for the next term in a Fourier expansion in order to obtain a nonzero result. This term is proportional to $\cos 4\theta$. However, it goes to zero for $\theta=\pi/8$, that is very near the location of the node in our specific model. This implies that the A_{1g} electronic response will be quite small at small energy, in contradiction with experiment, which shows a strong linear dependence. For a sizeable A_{1g} response at low energy, we need the zero of the A_{1g} Raman vertex and the node of the gap to be clearly apart. Since we have already chosen our order parameter, hence the node location, we achieve this by considering a more complicated Raman vertex, e.g., including the next order Fourier component: we take $\gamma_{A_{1g}}\sim A\cos 4\theta-(1-A)\cos 8\theta$. As seen in Fig. 12(b), we obtain a reasonably good agreement with experiment for $A=0.05$ and a small smearing $a=0.03$. We note that we are led to use different smearing for the different Raman symmetries, in contrast to what has been done in Ref. 16. This does not create a problem: the smearing is meant to account for lifetime effects at a phenomenological level. Hence, when dealing with different channels, there is no reason to have the same effective scattering. We obtain a sizeable contribution at low energy, at Δ_m and at Δ_M: this is clearly related to the fact that the Raman vertex is not small for $\theta=0$, for $\theta=\pi/4$ and at the node $\theta=\theta_0$. Note that, while the size of the low-frequency part is directly related to the strength of the Raman vertex around the node, the same is not true for the strength of the peaks at Δ_m and Δ_M. In particular, one may obtain a single broad bump between Δ_m and Δ_M instead of two peaks. This is naturally due to the complex effect of the screening term.

The small value $A=0.05$, which implies that the $\cos 4\theta$ contribution is negligible in the Raman vertex compared to the $\cos 8\theta$ contribution, comes from the strong constraints that the various characteristics of our A_{1g} spectrum put on the order parameter. We had already been led to consider a similar vertex in Ref. 16 to account for a A_{1g} spectrum that did not display a maximum at Δ_M. While this is not expected beforehand, this does not imply anything pathological about the Raman vertex we use and such a situation may very well occur accidentally. As we mentioned, we are merely led to this case by our request of a sizeable vertex at 0, $\pi/4$ and at the node. Clearly, we can achieve this goal in other ways if we allow more flexibility in our order parameter.

We demonstrate this by considering the following order parameter: $\Delta(\theta)=\Delta_M$ for $0<\theta<\theta_0-\Delta_M/S$, $\Delta(\theta)=S(\theta_0-\theta)$ for $\theta_0-\Delta_M/S<\theta<\theta_0+\Delta_m/S$, $\Delta(\theta)=-\Delta_m$ for $\theta_0+\Delta_m/S<\theta<\pi/4$. Its shape is similar to the simple one that we have used above, but in this way we can choose more freely the location of the node θ_0 of $\Delta(\theta)$ and its slope S. On the other hand, we restrict ourselves to the simplest Raman vertex $\gamma_{A_{1g}}\sim\cos 4\theta$. We find a reasonably good agreement with experiment [see Fig. 12(b)] for $\theta_0=35°$ and $S=3.6$. This shows that we can account for the A_{1g} spectrum by the simplest Raman vertex together with an order parameter having two maxima and a node. However, the bare B_{1g} spectrum provided by this latter order parameter has a very strong peak at Δ_M (inasmuch as we have taken a simple flat maximum model) and a quite small low-energy part, due to the node proximity of 45°. This cannot be reconciled with experiment by any reasonable smearing. Again, the strength of the linear low-energy part of the B_{1g} spectrum shows that the node is rather far away from 45°. Note however that we could cure somewhat this difficulty by assuming a more complicated B_{1g} Raman vertex, which would have a small strength for $\theta=0$ (in addition of being zero by symmetry for $\theta=\pi/4$). In conclusion, we believe that it is possible to account for experiment for all symmetries by an order parameter having the qualitative features that we have considered, together with Raman vertices reasonably close to the simplest one. This might require perhaps that we use a varying density of states, while here we have assumed it to be constant for simplicity. However, we have not tried to explore this problem more quantitatively.

Our model gives a natural explanation of the different positions of the B_{1g} and B_{2g} peaks and the existence of these two peaks in A_{1g} symmetry (even if screening complicates the matter). Note that peaks with different positions are also found in the other high-T_c superconductors (see Table I). At this point, we can notice that the existence of two electronic structures is not only detected in Raman scattering (see Table I) but also in Giaever tunneling[38] and spectroscopy tunneling measurements[39] in YBCO. The energies of these two structures were found at $\Delta = 20$ meV and $\Delta = 30$ meV, which corresponds to $2\Delta = 320$ and 480 cm^{-1}, respectively (very close to the values reported for YBCO in Table I). A $d+s$ wave model, as developed by Beal-Monod, Bleri and Maki,[40] accounts for the B_{2g} spectrum but cannot explain the A_{1g} and B_{1g} spectra unless one introduces a very large scattering rate, which is incompatible with our critical temperature as we have discussed above. We note finally that the high values of the maxima ($\sim 8-9 k_B T_c$) as well as the nonobservation of a significant softening of the maxima, as a function of the temperature, as reported in Sec. V.A, are incompatible with a weak coupling theory.[41]

VII. CONCLUSION

In conclusion, we have presented pure electronic Raman spectra of Hg-1223 single crystals. In the superconducting state our most significant results are (i) the two electronic maxima usually observed separately at 530 and 800 cm^{-1} in B_{2g} and B_{1g} symmetries respectively, are seen simultaneously in A_{1g} symmetry. The existence of such two electronic features at $2\Delta/k_B Tc = (5\text{-}6)$ and (8-9), are reported not only in Raman but also on tunneling measurements. (ii) these two electronic structures disappear at T_c without showing significant softening as the temperature is raised. (iii) the electronic response function exhibits an intrinsic linear ω dependence—not only in the B_{2g} spectrum—but also in the B_{1g} spectrum, which has been extensively studied in this work: the linear dependence is robust against the change of the excitation frequency, implying that this is an intrinsic feature arising from the gap symmetry. These experimental results strongly suggest a very anisotropic superconducting gap, involving two characteristic energies and nodes located away from the [110] and $[1\bar{1}0]$ directions. Such observations are inconsistent with a pure $d_{x^2-y^2}$ order parameter symmetry. The simplest order parameter compatible with our experimental data displays two maximum gap values and 8 nodes. It has the A_{1g} symmetry. We have developed a detailed comparison with the experimental spectra and we have shown that such an order parameter can account satisfactorily for our experimental results.

ACKNOWLEDGMENTS

We thank P. Monod, M. Cyrot, and G. Deutscher for very fruitful discussions. We are grateful to S. Poissonnet and L. Schmirgeld-Mignot for the chemical analysis by electron probe.

[1] D. A. Wollman, D. J. Van Harlingen, and D. M. Ginsberg, Phys. Rev. Lett. **74**, 797 (1995); C. C. Tsuei, J. R. Kirtley, Z. F. Ren, J. M. Wang, H. Raffy, and Z. Z. Li, Nature (London) **387**, 481 (1997).

[2] K. A. Koutnetzov, A. G. Sun, B. Cheu, A. S. Katz, S. R. Bahcall, John Clarke, R. C. Dynes, D. A. Gajewski, S. H. Han, M. B. Maple, J. Grapintzakis, J.-T. Kim, and D. M. Ginsberg, Phys. Rev. Lett. **79**, 3050 (1997); C. Rossel, H. Willemin, J. Hofa, H. Keller, Z. F. Ren, and J. H. Wang, Physica C **282–287**, 136 (1997).

[3] M. V. Klein and S. B. Dierker, Phys. Rev. B **29**, 4976 (1984).

[4] A. A. Abrikosov and V. M. Genkin, Zh. Eksp. Teor. Fiz. **65**, 842 (1973) [Sov. Phys. JETP **38**, 417 (1974)].

[5] S. B. Dierker, M. V. Klein, G. W. Webb, and Z. Fisk, Phys. Rev. Lett. **50**, 853 (1983).

[6] T. P. Devereaux, D. Einzel, B. Stadlober, R. Hackl, D. H. Leach, and J. J. Newmeier, Phys. Rev. Lett. **72**, 396 (1994); T. P. Devereaux and D. Einzel, Phys. Rev. B **51**, 16 336 (1995).

[7] S. L. Cooper, M. V. Klein, B. G. Pazol, J. P. Rice, and D. M. Ginsberg, Phys. Rev. B **37**, 5920 (1988); S. L. Cooper *et al.*, *ibid.* **38**, 11 934 (1988).

[8] R. Hackl, W. Gläser, P. Müller, D. Einzel, and K. Andres, Phys. Rev. B **38**, 7133 (1988); R. Hackl, in *Gap Symmetry and Fluctuations in High-T_c Superconductors*, Vol. 33 of NATO Advanced Study Institute, Series B: Physics, edited by J. Bok, G. Deutscher, D. Pavuna, and S. Wolf (Plenum, New York, 1998).

[9] T. Staufer, R. Nemetschek, R. Hackl, P. Müller, and H. Veith, Phys. Rev. Lett. **68**, 1069 (1992).

[10] D. H. Leach, C. Thomsen, M. Cardona, L. Mihaly, and C. Kendziora Solid State Commun. **88**, 457 (1993).

[11] R. Nemetschek, O. V. Misochko, B. Stadlober, and R. Hackl, Phys. Rev. B **47**, 3450 (1993).

[12] X. K. Chen, J. C. Irwin, H. J. Trodhal, T. Kimura, and K. Kishio, Phys. Rev. Lett. **73**, 3290 (1994).

[13] M. Krantz and M. Cardona, J. Low Temp. Phys. **99**, 205 (1995).

[14] L. V. Gasparov, P. Lemmens, M. Brinkmann, N. N. Kolesnikov, and G. Güntherodt, Phys. Rev. B **55**, 1223 (1997).

[15] T. Strohm and M. Cardona, Phys. Rev. B **55**, 12 725 (1997).

[16] A. Sacuto, R. Combescot, N. Bontemps, P. Monod, V. Viallet, and D. Colson, Europhys. Lett. **39**, 207 (1997).

[17] A. Sacuto and R. Combescot, in Ref. 8.

[18] A. Sacuto *et al.*, Physica C **259**, 209 (1996); X. Zhou *et al.*,Phys. Rev. B **55**, 12 770 (1997).

[19] M. Cantoni, A. Schilling, H.-U. Nisen, and H. R. Ott, Physica C **215**, 11 (1993).

[20] P. A. Wolff, Phys. Rev. **171**, 436 (1968); A. Kawabata, J. Phys. Soc. Jpn. **30**, 68 (1971).

[21] D. Colson, A. Bertinotti, J. Hammann, J.-F. Marucco, and A. Pinatel, Physica C **233**, 231 (1994); A. Bertinotti *et al.*, *ibid.* **250**, 213 (1995).

[22] A. Bertinotti, D. Colson, J-F. Marucco, V. Viallet, J. Le Bras, L. Fruchter, C. Marssenat, A. Carington, and J. Hammann, in *Studies of High Temperature Superconductors*, edited by A. Narlikar (Nova Science, New York, 1997).

[23] A. Carrington, D. Colson, Y. Dumont, C. Ayache, A. Bertinotti, and J. F. Marucco, Physica C **234**, 1 (1994).
[24] A. Sacuto, C. Julien, V. A. Shchukin, C. Perrin, and M. Mokhtari, Phys. Rev. B **52**, 7619 (1995).
[25] R. M. Macfarlane, H. J. Rosen, E. M. Engler, R. D. Jacovitz, and V. Y. Lee, Phys. Rev. B **38**, 284 (1988).
[26] A. El Azrak, Ph.D. thesis, Université Paris-Sud, 1993.
[27] S. L. Cooper *et al.*, Phys. Rev. B **47**, 8233 (1993).
[28] S. Uchida *et al.*, Phys. Rev. B **43**, 7942 (1991).
[29] I. Terasaki *et al.*, Physica C **165**, 152 (1990).
[30] T. P. Devereaux, J. Supercond. **8**, 421 (1995); T. P. Devereaux *et al.*, Phys. Rev. Lett. **72**, 3291 (1994).
[31] Moonsoo Kang, G. Blumberg, M. V. Klein, and N. N. Kolesnikov, Phys. Rev. Lett. **77**, 4434 (1996).
[32] T. P. Devereaux, Phys. Rev. Lett. **74**, 4313 (1995).
[33] G. Preosti, H. Kim, and P. Muzikar, Phys. Rev. B **50**, 1259 (1994).
[34] J. Annett, N. Goldenfeld, and S. R. Renn, Phys. Rev. B **43**, 2778 (1991).
[35] P. J. Hirschfeld, W. O. Putikka and D. J. Scalapino, Phys. Rev. B **50**, 10 250 (1994).
[36] D. A. Bonn *et al.*, Phys. Rev. B **50**, 4051 (1994).
[37] S. Hensen, G. Müller, C. T. Rieck, and K. Scharnberg, Phys. Rev. B **56**, 6237 (1997).
[38] I. Maggio-Aprile, C. Renn, A. Erb, E. Walker, and O. Fischer, Phys. Rev. Lett. **75**, 2754 (1995).
[39] G. Deutscher in Ref. 8.
[40] M. T. Beal-Monod, J. B. Bieri, and K. Maki, Europhys. Lett. **40**, 201 (1997); N. Nemetschek *et al.* (unpublished).
[41] R. Combescot, cond-mat/9710115 (unpublished).